Bioorganic Chemistry 141 (2023) 106838

Contents lists available at ScienceDirect

Bioorganic Chemistry

journal homepage: www.elsevier.com/locate/bioorg

In *vitro* and in *vivo* anticancer activity of novel Rh(III) and Pd(II) complexes with pyrazolopyrimidine derivatives

Yun-Qiong Gu [a,b,1], Meng-Xue Ma [a,1], Qi-Yuan Yang [a,b], Kun Yang [a], Huan-Qing Li [a], Mei-Qi Hu [a], Hong Liang [a,*], Zhen-Feng Chen [a,*]

[a] *State Key Laboratory for Chemistry and Molecular Engineering of Medicinal Resources, Key Laboratory for Chemistry and Molecular Engineering of Medicinal Resources (Ministry of Education of China), Collaborative Innovation Center for Guangxi Ethnic Medicine, School of Chemistry and Pharmaceutical Sciences, Guangxi Normal University, Guilin 541004, China*

[b] *School of Environment and Life Science, Nanning Normal University, Nanning 530001, China*

ARTICLE INFO

Keywords:
Rh(III)/Pd(II) complexes
Anticancer activity
Cell cycle arrest
ER-stress
Apoptosis

ABSTRACT

Six pyrazolopyrimidine rhodium(III) or palladium(II) complexes, $[Rh(L^1)(H_2O)Cl_3]$ (**1**), $[Rh(L^2)(CH_3OH)Cl_3]$ (**2**), $[Rh(L^3)(H_2O)Cl_3]$ (**3**), $[Rh_2(L^4)Cl_6]\cdot CH_3OH$ (**4**), $[Rh(L^5)(CH_3CN)Cl_3]\cdot 0.5CH_3CN$ (**5**), and $[Pd(L^5)Cl_2]$ (**6**), were synthesized and characterized. These complexes showed high cytotoxicity against six tested cancer cell lines. Most of the complexes showed higher cytotoxicity to T-24 cells *in vitro* than cisplatin. Mechanism studies indicated that complexes **5** and **6** induced G2/M phase cell cycle arrest through DNA damage, and induced apoptosis *via* endoplasmic reticulum stress response. In addition, complex **5** also induced cell apoptosis *via* mitochondrial dysfunction. Complexes **5** and **6** showed low *in vivo* toxicity and high tumor growth inhibitory activity in mouse tumor models. The inhibitory effect of rhodium complex **5** on tumor growth *in vivo* was more pronounced than that of palladium complex **6**.

1. Introduction

Cancer has become one of the main causes of disease death, which is caused by the abnormal proliferation of cells that grow out of control in the body. It involves cross-talk among multiple genes and signaling pathways, DNA alterations, gene transcription and translation [1,2] and it is an extremely complicated and highly lethal disease [3–5]. Metal-based drugs such as cisplatin and its analogues have been widely used to treat different types of cancer for more than 40 years [6], including ovarian, bladder, cervical, testicular, and lung cancers, as well as lymphoma, myeloma, and melanoma [7–11]. However, cisplatin has serious toxicity and often develops drug resistance [12]. Thus, overcoming these disadvantages has become a top priority in the development of metal-based antitumor drugs through the discovery of agents with stronger antitumor activity, less toxic side effects and lower tendency to induce drug resistance [13].

Among them, rhodium(III) and palladium(II) complexes have attracted much interest due to their unique chemical and pharmacological properties [14–16]. The rhodium complexes exhibit a variety of biological activities [17–19], such as anticancer [20], antibacterial [21] and antifungal activities [22]. The different modes of interactions between Rh(III) complexes and biomolecular targets may be related to their unique molecular structures [23,24]. Various rhodium polypyridine complexes bind DNA via covalent and noncovalent interactions, to improve the uptake of the drug by cells and enhance cytotoxicity by increasing the rigid plane and hydrophobicity of the polypyridine ligand [25]. Quercetin rhodium(III) complex exhibits potent anti-proliferative activity and a higher safety profile for normal cells, through triggering apoptosis and causing cell cycle arrest in the sub G0 phase [26]. Palladium(II) complexes efficiently bind to HSA (human serum albumin) molecules, revealing a rational model for anticancer drug design, transport, and toxicity reduction [27]. These rhodium and palladium complexes have shown significant anticancer activities with few side effects and they have the potential to be developed as platinum drug substitutes.

Our previous studies have found that Rh(III)/Pd(II) complexes with isoquinoline derivatives induced HepG2 cell death by mitochondria-mediated apoptotic and autophagic pathways [28]. Some rhodium

* Corresponding authors.
E-mail addresses: hliang@gxnu.edu.cn (H. Liang), chenzf@gxnu.edu.cn (Z.-F. Chen).
[1] Yun-Qiong Gu and Meng-Xue Ma contributed equally to this work.

https://doi.org/10.1016/j.bioorg.2023.106838
Received 23 July 2023; Received in revised form 22 August 2023; Accepted 4 September 2023
Available online 16 September 2023

(III)-picolinamide complexes inhibited cell proliferation through multiple modes of action including cell cycle arrest, apoptosis autophagy, and metastasis suppression[24]. And the ruthenium(III) complexes of pyrazopyrimidine derivative showed strong anti-proliferation activity against cancer cells [29]. These results suggested that more bioactive metal complexes could be designed by coordination of bioactive ligands with bioactive metal center. Pyrazopyrimidine scaffolds are one of the privileged heterocycles in drug discovery, which is the main structural component of many lead molecules. Because pyrazopyrimidine is similar to the adenine base in DNA, its fingerprint as a pharmacophore has always attracted attention [30,31]. However, there are few reports on the metal complexes with pyrazopyrimidine derivative and their antitumor effects. Herein, we synthesized highly active and low toxic rhodium/palladium metal complexes by coordinating pyrazolopyrimidine derivatives with good antitumor activity with bioactive rhodium/palladium metal centers, and their antitumor mechanisms were explored.

2. Results and discussion

2.1. Synthesis and characterization

Complexes $[Rh(L^1)(H_2O)Cl_3]$ (**1**), $[Rh(L^2)(CH_3OH)Cl_3]$ (**2**), $[Rh(L^3)(H_2O)Cl_3]$ (**3**), $[Rh_2(L^4)Cl_6]\cdot CH_3OH$ (**4**), $[Rh(L^5)(CH_3CN)Cl_3]\cdot 0.5CH_3CN$ (**5**), and $[Pd(L^5)Cl_2]$ (**6**) were characterized by single crystal X-ray diffraction analysis (Fig. 1). Complexes **1**, **2**, **3**, **5**, and **6** had a mononuclear structure with a 1:1 metal to ligand ratio. The central Rh(III) coordinated with two N atoms of the pyridine and pyrazole rings of the ligands, three chloride ions, and an O or N atom of a solvent molecule (H_2O molecules for complexes **1** and **3**, methanol for **2** and acetonitrile for **5**) to form a distorted octahedral geometry. However, complex **4** was a binuclear structure with a metal to ligand ratio of 2:1. The two rhodium(III) centers formed a six-coordinated distorted octahedral geometry connected by two μ^2-Cl. One Rh(III) center had the same coordination pattern as the other rhodium complexes, and the other Rh(III) center coordinated with the N atom of the pyrazole ring and a C atom of the benzene ring as well as two free chloride ions. The central Pd(II) ion of complex **6** was chelated with two N atoms of the pyridine and pyrazole rings of the ligands, two chloride anions to forms a four-coordinated square planar geometry. The crystallographic information of complexes **1**–**6** is shown in Table S1.

2.2. Stability, purity and log $P_{O/W}$ determination of the complexes

The stability of complexes **1**–**6** was measured by HPLC (Fig. S16) and UV − Vis spectroscopy (Fig. S17). The complexes showed no new peak within 48 h by HPLC, and the peak retention time hardly changed, indicating that the complexes were stable for at least 48 h at room temperature in solution. In addition, HPLC also showed that the purity of the complexes was above 98%, which could be used for further cell experiments [32]. Meanwhile, the absorption peaks and shapes of the UV spectra of these two complexes were unchanged over 72 h, indicating that complexes **1**–**6** were stable in PBS solution for at least 72 h, which is consistent with the HPLC results [33]. Furthermore, the complexes were dissolved in deionized water (1 mg complex/5mL H_2O) and LC-MS analysis was performed after 48 h. The mass spectra are shown in Fig. S18 − S22: For complex **1** (Fig. S18) $C_{17}H_{20}Cl_3N_6ORh$: HRMS (CH_3OH, *m/z*): calcd for $[M-H_2O+Na]^+$: 536.9611, found, 536.9620; calcd for $[M+Na]^+$: 554.0717, found, 554.9723. For complex **2** (Fig. S19) $C_{26}H_{38}Cl_3N_6ORh$: HRMS (CH_3OH, *m/z*): calcd for $[M-CH_3OH+Na]^+$: 649.0863, found, 649.0876. For complex **3** (Fig. S20) $C_{25}H_{36}Cl_3N_6ORh$: HRMS (CH_3OH, *m/z*): calcd for $[M-H_2O+Na]^+$: 649.0843, found, 649.0868. For complex **4:** The solubility of the complex in water was too poor to be detected. For complex **5** (Fig. S21) $C_{29}H_{25}Cl_3N_7Rh$: HRMS (CH_3OH, *m/z*): calcd for $[M+Na]^+$: 660.9924, found, 660.9927. For complex **6** (Fig. S22) $C_{27}H_{22}Cl_2N_6Pd$: HRMS (CH_3OH, *m/z*): calcd for $[M-Cl]^+$: 571.0629, found, 571.0626. These results indicated that these complexes were stable in aqueous solution for at least 48 h.

Lipophilicity is a physicochemical property of a drug which affects its uptake, metabolism and molecular toxicity [34]. To determine the lipophilicity of the complexes, log $P_{o/w}$ values (*N*-Octanol/water partition constant) of complexes **1**–**6** were measured (Fig. S23). It was found that the log $P_{o/w}$ values of complexes **1** and **4** were negative, -0.50 ± 0.05 and -0.45 ± 0.06, respectively, indicating that these two complexes are hydrophilic. The log $P_{o/w}$ values of the remaining complexes were positive, and increased in the order of complex **5** > complex **2** > complex **6** > complex **3**, indicating that they are lipophilic complexes, and

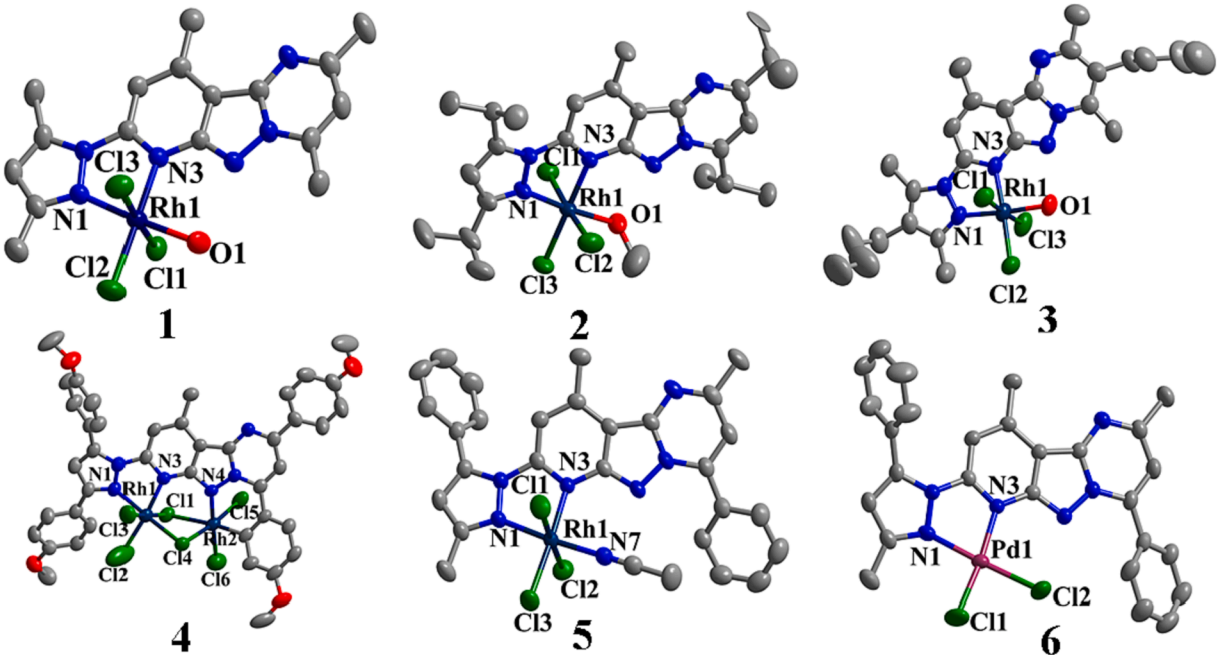

Fig. 1. Crystal structures of complexes **1**–**6**.

complex **5** is the most lipophilic, with a log $P_{o/W}$ value of 0.50±0.10 [35,36].

2.3. Cytotoxicity of the complexes

The cytotoxic activities of two new ligands ($\mathbf{L^2}$ and $\mathbf{L^4}$), six complexes **1**–**6** and cisplatin were investigated *in vitro* against five human tumor cell lines (T-24, A549, BEL-7404, HeLa, SK-OV-3 cells) and two normal cell lines (WI38 and HL-7702) by MTT assay (Table 1). The IC_{50} values of the complexes against tested cell lines were <20 μM except for complexes **1** and **4**, which may be due to their low solubility. Overall, complex **5** was the most cytotoxic compound in all cancer cell lines tested, with IC_{50} values 2–6 times lower than that of cisplatin. All complexes showed the highest anti-proliferation activity against T-24 cell lines, especially complex **5**, whose IC_{50} value was 2.1±0.1 μM. The activity of complex **6** with the same ligand as complex **5** against T-24 was lower than that of complex **5**, and its IC_{50} value was only 8.8±0.3 μM. For the other cell lines, the same trend was observed, and the selectivity index (**SI** = IC_{50} (HL-7702)/IC_{50} (T-24) of the complexes was higher than that of cisplatin. The cytotoxic activity of rhodium complexes with similar coordination pattern is correlated with their ligands for T-24 cancer lines: (1) When R_1 and R_2 of the pyrazole ring are R_1 = R_2 = $-CH_3$ and the pyrazole ring R_3= $-(CH_2)_3CH_3$, the anti-proliferation activity of the corresponding complex **3** was significantly enhanced than that of complex **1** (R_3 = −H). When the methyl groups of $R_1 = R_2 = -CH(CH_3)_2$ and R_3 = H, the anti-proliferation activity of the corresponding complex was also significantly enhanced, e.g. complex **2** > complex **1**, but complex **2** < complex **3**; (2) When R_1 = − Ph, R_2 = $-CH_3$ and R_3 = − H in complex **5**, it was the most cytotoxic complex. Therefore, complexes **5** and **6** with different metal centers of the same ligand were selected to further study the mechanism of their anti-proliferation effects on T-24 cells.

2.4. Cellular uptake and distribution of the complexes

The cellular uptake of metal anticancer drugs is a crucial factor affecting their anti-proliferation activity [37]. To investigate the kinetics of cellular uptake of complexes **5** and **6**, ICP-MS was used to measure their uptake in T-24 cells. The results showed that the concentration of rhodium uptake of complex **5** was 859.72±72.97 ng/10^6 cells after treatment at 15 μM for 10 h. The uptake of palladium in complex **6** by cells was 296.84±45.66 ng/10^6 cells (Fig. S24A and B). The uptake of complexes by cells affects their anti-proliferative activity against tumor cells, and previous studies have shown that the distribution of the complexes in subcellular organelles is closely related to different cellular pathways [38]. The distribution of complex **5** rhodium metal in the subcellular compartment was studied (Fig. S24C). Of all the subcellular compartments measured, the uptake into cytoplasm was the highest, followed by mitochondria and nucleus, and cell membrane was the lowest. These experiments indicated that complex **5** was accumulated in the mitochondria and nuclei of cancer cells, and likely causes damage to these two organelles.

2.5. Effects of complexes 5 and 6 on gene transcription levels in T-24 cells

To investigate the cytotoxicity mechanism of complexes **5** and **6**, we first investigated the transcription levels of genes involved in common cell death pathways using high-sensitivity single-cell RNA sequencing (RNA-SEQ). After the complexes were incubated with T-24 cancer cells for 24 h, total RNA was extracted and the relevant gene transcript levels were analyzed (Fig. 2). The results showed that complexes **5** and **6** affected the apoptosis and DNA pathway related genes. They activated the expression of Bax, Bad, Bcl-2 and Caspase 2/3 genes and disrupted the expression of other apoptosis-related genes in T-24 cells (Fig. 2A). At the same time, the expression levels of DNA damage-related genes DRAM2, DDIT4, GADD45A/G, XPA/C, CCI2, DDB1 and MDC1 were also changed (Fig. 2B). The results showed that complexes **5** and **6** may induce apoptosis and DNA damage of T-24 cancer cells by regulating the expression of related genes, thereby inhibiting the proliferation of T-24 cells.

2.6. The comet experiment, cell cycle arrest and the expression levels of cycle-related proteins

DNA has been demonstrated as the main molecular target of various metal complexes [39,40]. Therefore, we evaluated the DNA damage by complexes **5** and **6** first. After treatment with complexes **5** and **6** for 24 h, DNA fragments of T-24 cells were assessed by basic single-cell gel electrophoresis (comet assay) (Fig. 3A and B). The results showed that treatment of T-24 cells with **5** and **6** increased the electrophoretic migration of DNA fragments. The single cell DNA showed the pattern of a comet, and the tail length of comet was longer than that of the control cell, showing a “broom” pattern of tail. Moreover, the effect of complex **5** on DNA damage was concentration-dependent, indicating that complexes **5** and **6** induced DNA damage in cells. As a result, cell cycle arrest and apoptosis could be induced [41].

The cell cycle is a highly ordered process in cell growth, tissue regeneration, DNA repair, and apoptosis [42]. Among the cell cycle, interphase is mainly composed of three stages: G1, G2 and S [43,44]. At the concentration of 4.0 μM, both complexes **5** and **6** induced G2/M phase arrest in T-24 cells, and the arrest effect of complex **5** was more obvious than that of complex **6**. Moreover, the proportion of cells in G2/M phase increased from 12.34% (control) to 44.96% and 25.18%, respectively, after treatment with complexes **5** and **6** (Fig. 3C). After T-24 cells were treated with complex **5** (2.0, 3.0 and 4.0 μM) for 24 h, the proportion of G2/M phase cells increased from 20.16% to 44.21% and the proportion of S and G1 phases cells decreased (Fig. 3D).

Phosphorylated cyclin p-CDC25C^{s216} (60 KDa) is one of the DNA damage-mediated G2 phase checkpoints in cell cycle progression. Cyclin-dependent protein kinases (CDKs) are a group of serine/

Table 1
The cytotoxicity of ligands, metal salts and complexes **1**–**6** against five human tumor cell lines and two normal cell lines by MTT method (IC_{50}[a], 48 h).

Compound	T-24	A549	BEL-7404	HeLa	SKOV-3	WI38	HL-7702	SI
L^4	>20	>20	>20	>20	>20	>20	>20	–
L^5	>20	>20	>20	>20	>20	>20	>20	–
1	>20	>20	>20	>20	>20	>20	>20	–
2	8.2±0.8	10.9±0.4	15.5±0.9	15.3±0.8	18.0±0.1	9.3±1.6	13.0±0.8	1.6
3	4.3±0.5	5.6±0.4	7.4±0.2	8.5±0.8	9.3±0.1	5.1±0.8	7.4±1.0	1.7
4	>20	>20	>20	>20	>20	>20	>20	–
5	2.1±0.1	4.5±0.4	5.7±0.9	4.2±0.4	5.8±0.2	3.2±0.3	2.5±0.3	1.2
6	8. 8±0.3	12.4±0.5	14.4±0.9	12.3±0. 3	12.9±0.8	14.0±0.8	16.9±0.3	1.9
DDP	11.0±0.5	11.4±0.5	34.2±0.7	16.6±0.5	8.0±1.0	7.4±0.6	9.3±0.50	0.8
$RhCl_3{\cdot}3H_2O$	>40	>40	>40	>40	>40	>40	>40	–
$PdCl_2$	>40	>40	>40	>40	>40	>40	>40	–

[a] IC_{50} values are expressed as the mean ± standard deviation of three independent experiments. **SI** (Selectivity indices) = IC_{50}(HL-7702)/IC_{50}(T-24).

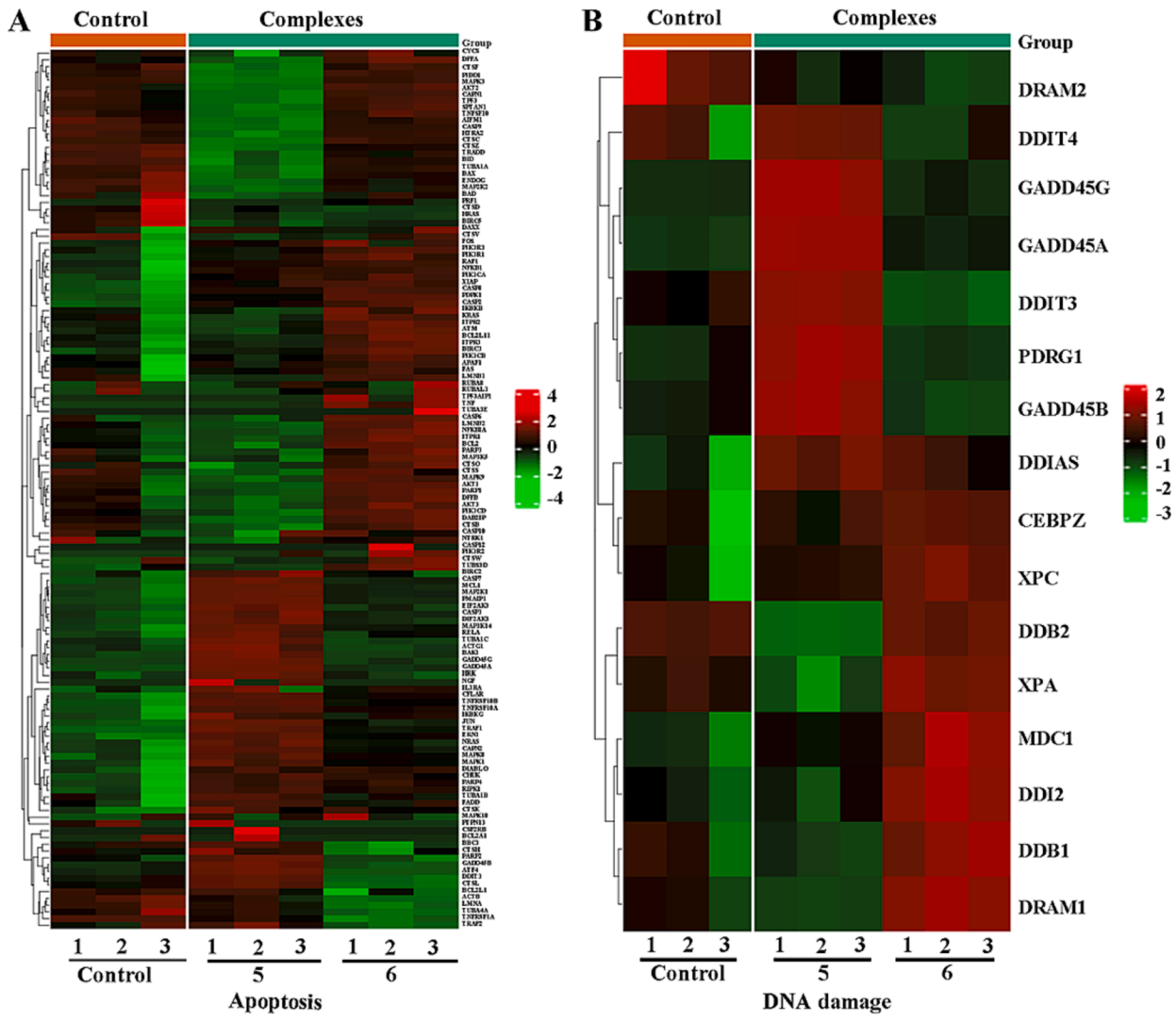

Fig. 2. Effects of complexes **5** and **6** on the transcription levels of genes associated with DNA damage (A), apoptosis (B) in T-24 cells.

threonine protein kinases that drive the cell cycle through their chemotactic effects on serine/threonine proteins. The cyclin-CDK complex, through CDK activity, catalyzes the phosphorylation of different substrates to achieve the advancement and transformation of different phases of the cell cycle [45]. Our experimental results demonstrated that the cyclin p-CDC25C^{S216} was significantly increased, and CDK2 and Cyclin B1 were significantly decreased in the complexes-treated group compared with the control, indicating that the G2/M phase arrest of T-24 cells by complexes **5** and **6** may be achieved by regulating the expression of CDK2, Cyclin B1 and p-CDC25C [46], which are in good agreement with the flow cytometry results (Fig. 3E and F).

2.7. Cell apoptosis and the expression levels of apoptosis-related proteins

Cell cycle arrest also seriously affects tumor cell apoptosis [47], therefore we further evaluated the apoptosis induced by complexes **5** and **6** with Annexin V and PI staining. In Fig. 4, the apoptosis rates (Q2 + Q3) of cells treated with these two complexes for 24 h at the concentration of 4.0 μM were 28.05% and 13.69%, respectively (Fig. 4A). When treated with the complexes for 48 h, the apoptosis rates (Q2 + Q3) were 71.1% and 24.54% (Fig. 4B), respectively, indicating that complexes **5** and **6** increased the percentage of apoptosis and obviously induced apoptosis of T-24 cells. Moreover, the percentage of apoptosis induced by complex **5** was concentration-dependent after different concentrations of complex **5** were applied to cells for 24 h (Fig. S25). The results clearly confirmed that complexes **5** and **6** effectively induced cell apoptosis in a time-and concentration-dependent manner[48], and the apoptosis rate was higher than that of cisplatin at the same concentration.

Bcl-2 family of proteins is the dominant regulator of the normal apoptotic process, and is also a major player in tumorigenesis, progression and resistance to subsequent drug therapy mediated by apoptotic escape [47], which includes enhancing apoptosis protein (Bad and Bax) and decreasing antiapoptotic proteins (Bcl-2). To confirm the apoptosis induced by complexes **5** and **6**, the change of Bax and Bcl-2 were assayed by Western blot. The experimental results showed that Bax protein expression was elevated and Bcl-2 protein expression was decreased compared with the control (Fig. 4C and D). This result indicated that complexes **5** and **6** induced T-24 cells apoptosis (Fig. 4C and D).

2.8. Complex 5 induces mitochondrial dysfunction

We investigated the effect of complex **5** on mitochondrial function. Mitochondrial membrane potential (MMP, ΔΨm) is a fundamental feature reflecting mitochondrial integrity [49]. Mitochondrial depolarization induced by complex **5** was detected by JC-1 kit staining by flow cytometry. After treatment with complex **5** (2.0, 3.0 and 4.0 μM) for 24

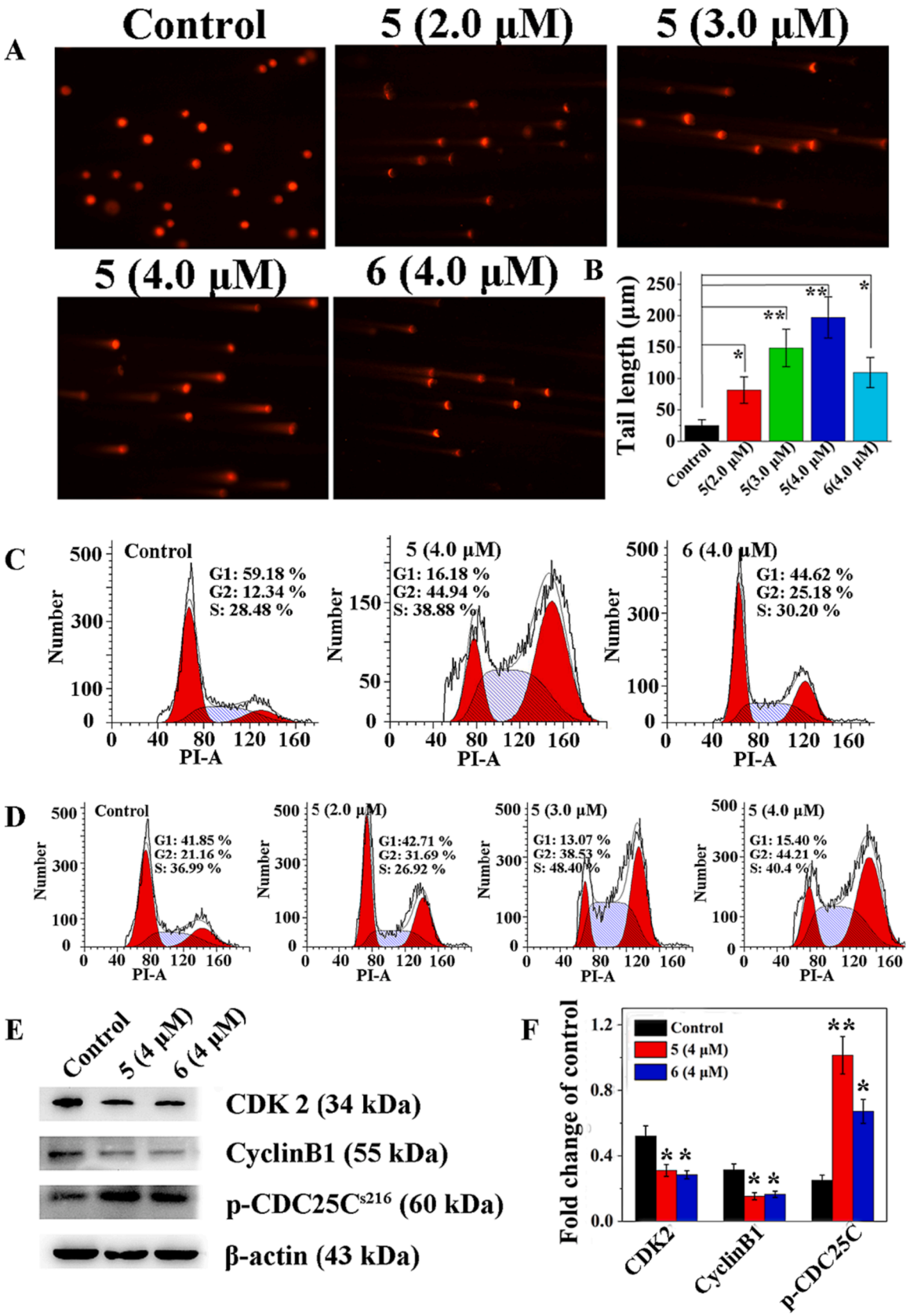

Fig. 3. (A) The comet assay was imaged by fluorescence microscopy with EB-staining after incubation with **5** and **6** for 24 h on T-24 cells (400×). (B) The tail length of the cells in each treated group was measured by the comet assay Effects on the cell cycle after treated with complexes **5** (4.0 μM), **6** (4.0 μM) (C) and **5** (2.0, 3.0 and 4.0 μM) (D). (E) Effect of complexes **5** and **6** on cycle-related proteins in T-24 cells for 48 h. (F) Histograms display the density ratios of cell cycle related proteins (***P < 0.001, **P < 0.01, *P < 0.05).

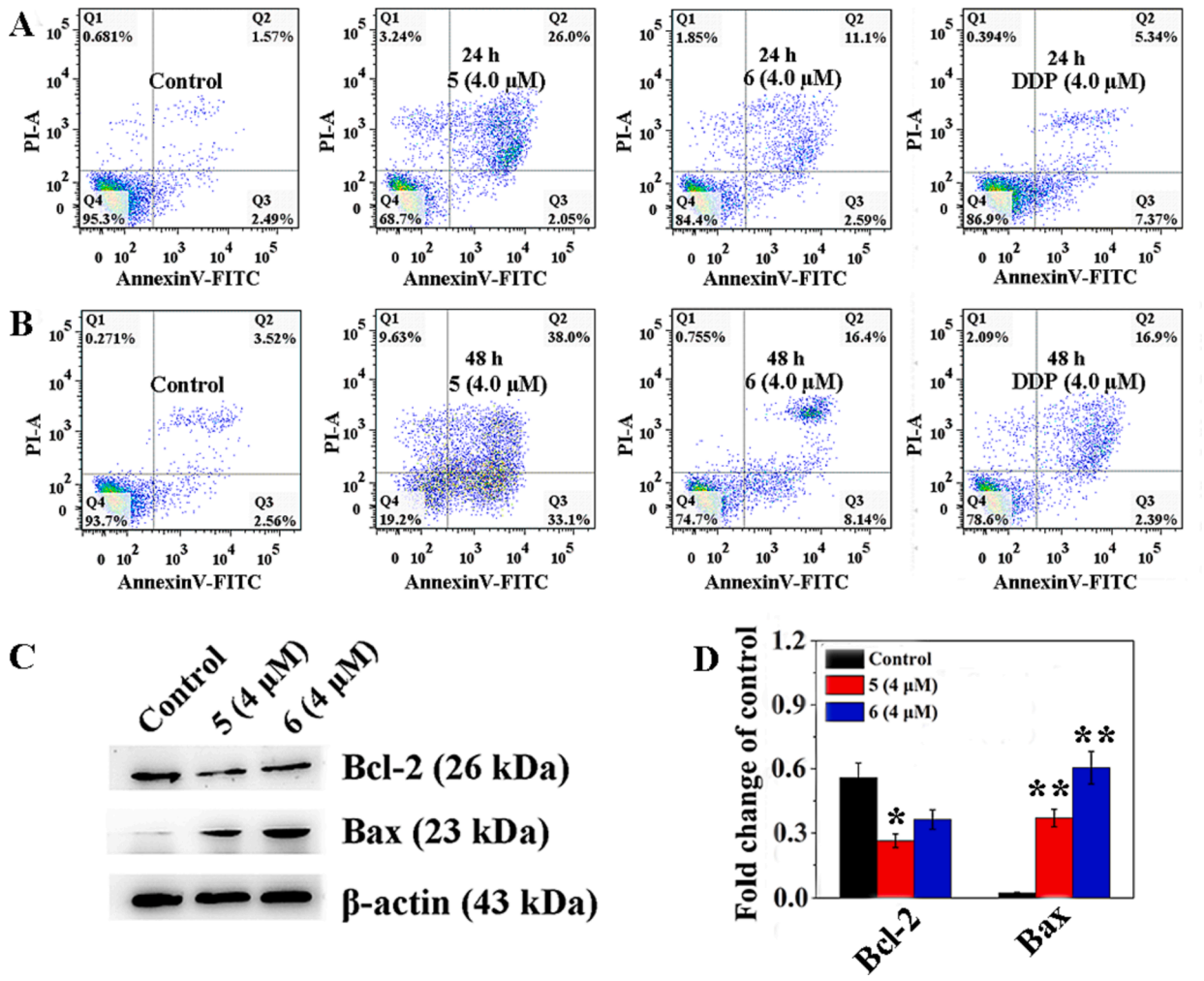

Fig. 4. Effect of complexes **5** and **6** on cell apoptosis of T-24 cells for 24 h (A) or 48 h (B). (C) Effect of complexes **5** and **6** on apoptosis-related proteins in T-24 cells for 48 h (D) Histograms display the density ratios of apoptosis elated proteins (***P < 0.001, **P < 0.01, *P < 0.05).

h, mitochondrial membrane potential was decreased to 6.94%, 32.2% and 33.9% compared with the control cells (Fig. 5A), which indicated cell mitochondrial membrane may be damaged by the complex [50].

The production of intracellular reactive oxygen species (ROS) is a crucial indicator in the induction of apoptosis in multifarious cell lines [51]. Since the mitochondria are the main source of ROS, mitochondrial function damage often leads to increased ROS levels and calcium levels [52]. To investigate whether complex **5** would alter the intracellular ROS levels, we first investigated the intracellular ROS levels treated with complex **5** by 2′,7′-dichlorodihydrofluorescein diacetate (H_2DCF-DA) staining. After treatment with complex **5** for 10 h, a concentration dependent enhancement of green fluorescence intensity was observed in complex **5**-treated T-24 cells, indicating an increase in intracellular ROS (Fig. 5B). At the same time, we also determined the intracellular calcium and ATP levels, and found that calcium content increased in a concentration-dependent manner (Fig. 5C), while ATP level decreased significantly (Fig. 5D).

A decrease in MMP indicates a shift in mitochondrial permeability. This phenomenon leads to uncoupling of the respiratory chain, resulting in cessation of ATP synthesis, ROS overproduction, and decreased ATP [53]. ROS overproduction and ATP depletion in turn promote mitochondrial dysfunction, leading to rupture of mitochondrial outer membrane and release of apoptotic factors [50]. We found cascade changes in mitochondria following complex **5** treatment, such as decreased MMP, increased ROS and Ca^{2+} accumulation, and decreased ATP levels [54]. These findings are consistent with an increased rate of cell apoptosis. In conclusion, mitochondria dependent apoptosis is the cause of apoptosis induced by complex **5** [14]. Without sufficient ATP produced by mitochondria, the rapid proliferation of cancer cells is hampered, which is also consistent with previous conclusions.

2.9. Complexes 5 and 6 induce endoplasmic reticulum stress

Many studies show that ROS production is an important component of ER stress responses and may act as an upstream signal [55]. The effects of complexes on ER stress were examined by ER-Tracker dyes. The green fluorescence of ER-Tracker was significantly enhanced as shown by confocal fluorescence photography after cells were incubated with complexes **5** and **6** (Fig. 6A), indicating that these two complexes induced ER stress in T-24 cancer cells [56].

ER is the major store of intracellular Ca^{2+} which is an important marker of cell signaling and survival [57]. When physiological changes of ER occur, Ca^{2+} is released into the cytoplasm [58]. Several ER stress pathways exist in mammalian cells [59]. Elevated expression levels of p-PERK (Phosphorylated RNA-dependent protein kinase-like endoplasmic reticulum kinase), p-eIF2α (phosphorylated eukaryotic promoter 2α), and CHOP (nuclear transcription factor C/EBP homologous protein) indicated ER stress [60]. To verify whether **5** and **6** could induce ER stress, the expression levels of endoplasmic reticulum stress signature proteins p-PERK, P-eIF2α and CHOP in **5** and **6** treated cells were

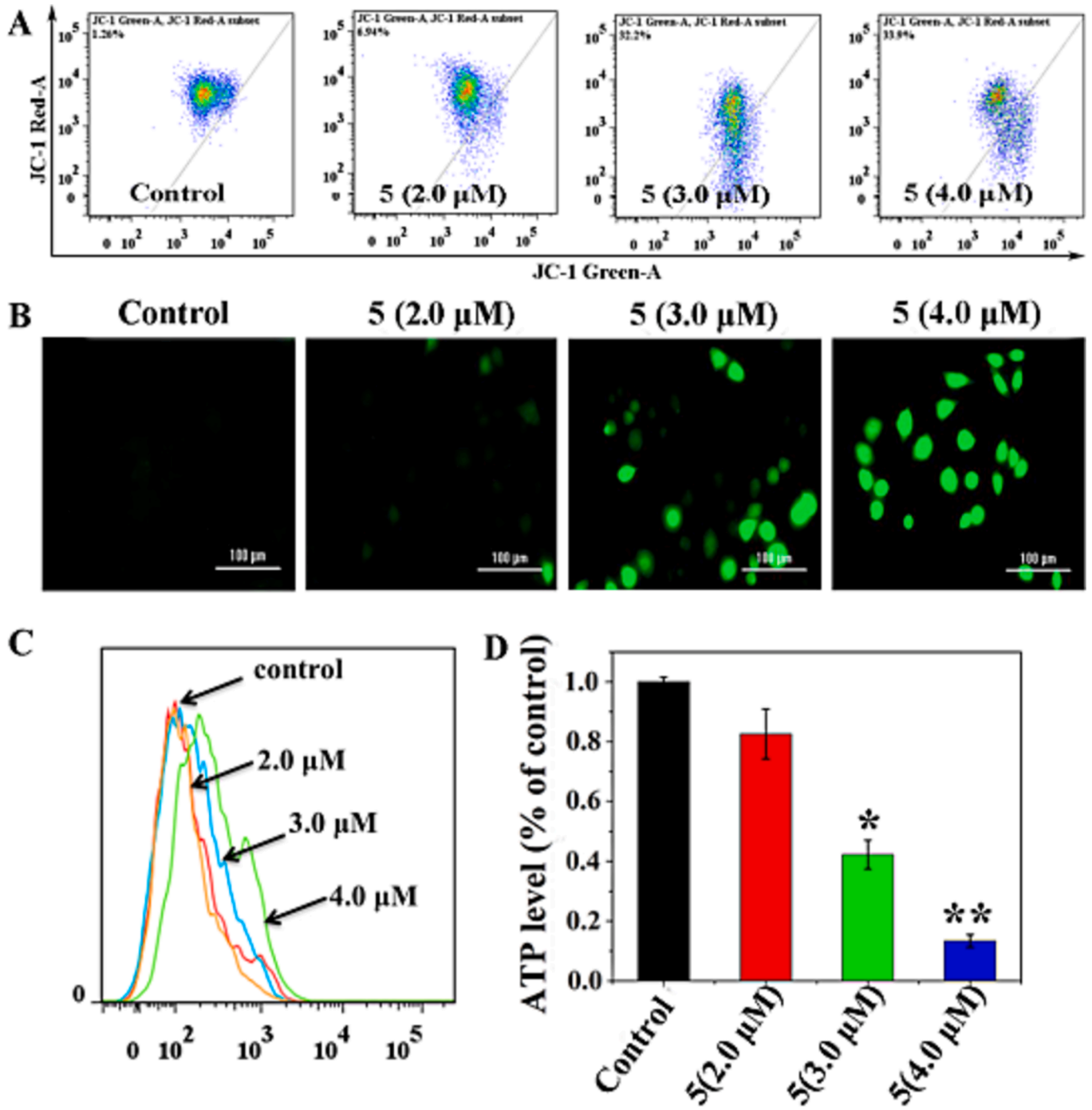

Fig. 5. (A) The influence of complex **5** on mitochondrial membrane potential in T-24 cells (24 h). (B) The ROS determination of cells after incubation of complex **5** (10 h). (C) The measurement of Ca^{2+} release in the cells upon treatment with complex **5** (24 h). (D) The detection of the intracellular ATP level after incubation of complex **5** (24 h) (***P < 0.001, **P < 0.01, *P < 0.05).

detected by Western blot. Complexes **5** and **6** were found to significantly increase the expression of p-PERK, P-eIF2α and CHOP proteins (Fig. 6B and C), indicating an increased level of ER stress [61].

2.10. Complexes 5 and 6 activate caspase 3/8/9

In general, there are two different pathways involved in the apoptosis of cancer cells, the intrinsic pathway (mitochondria-related apoptosis pathway) and the extrinsic pathway [50]. The intrinsic pathway is typically dependent on the activation of the initiator caspase-9 and caspase-3 [62]. Moreover, CHOP interacts with the death receptor 5 (DR5) promoter and is activated by caspase-8 to induce the death receptor apoptosis pathway [63,64].

To explore the complex **5**-induced apoptosis pathway, we first detected the activation of caspase-3/8/9 by complex **5** in T-24 cells. Complex **5**-treated cells showed additional peaks in activated caspase-3/8/9 cells compared with untreated cells (Fig. 7). After treatment with complex **5**, the proportion of activated caspase-3/8/9 cells in total T-24 cells was 36.70%, 23.00% and 32.37%, respectively, which showed obvious concentration dependence. These results suggested that complex **5** activated caspase-3/8/9 in T-24 cells, thereby inducing apoptosis mediated by mitochondrial dysfunction [65].

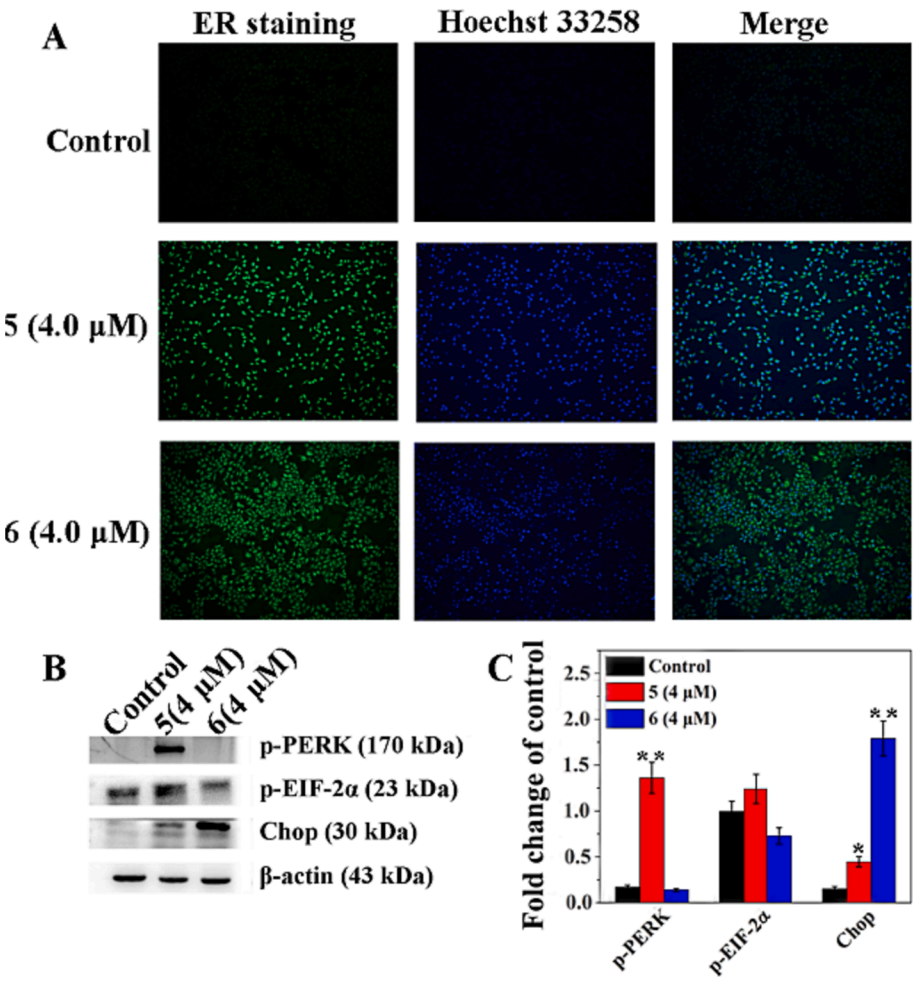

Fig. 6. (A) Confocal micrographs of cells after treatment with ER-Tracker staining (green) and Hoechst 33,258 staining (blue). (B) Effect of complexes **5** and **6** on ER-stress-related protein against T-24 cells for 48 h. (C) Histograms display the density ratios of ER-stress-related proteins (***P < 0.001, **P < 0.01, *P < 0.05). (For interpretation of the references to colour in this figure legend, the reader is referred to the web version of this article.)

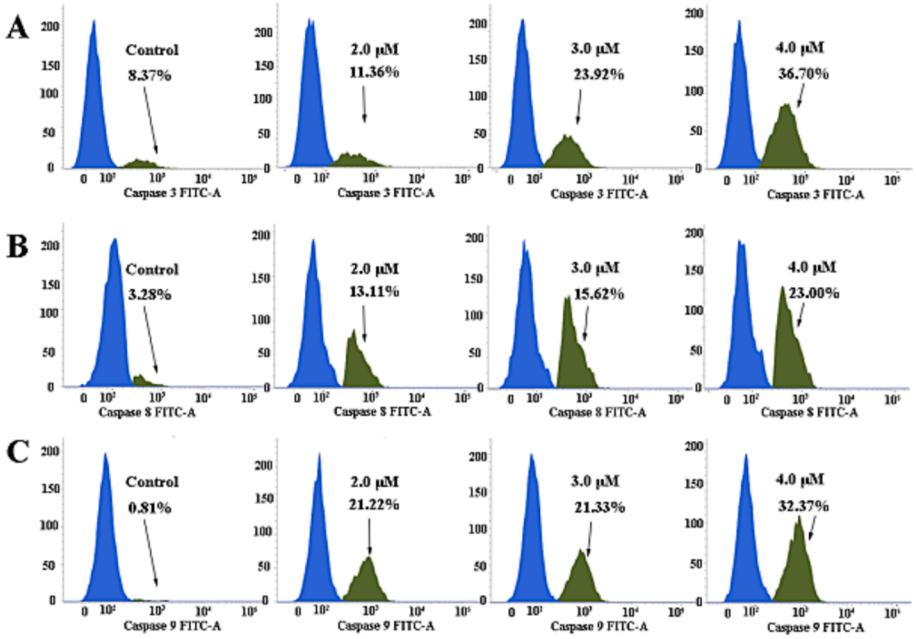

Fig. 7. The activation of caspase-3/8/9 (A, B and C) in T-24 cells after incubation with complex **5** (24 h).

2.11. In vivo anticancer activity in xenograft tumor model

Acute toxicity test showed that the safe dose of complexes **5** and **6** was 30 mg/kg after a single caudal vein injection, and both groups of mice survived.

The *in vivo* anticancer activity of complexes **5** and **6** was studied using T-24 cell xenograft mouse model. When the tumor volume was suitable (about 90 mm^3), the mice were divided into 4 groups randomly (n = 6) and were treated with vehicle, complex **5** (30 mg/kg), complex **6** (30 mg/kg) and DDP (2 mg/kg), respectively. Intraperitoneal injections are given every 2 days. Tumor size was measured every 2 days after treatment (Fig. 8A). At the end of treatment on the 15th day, the tumor weight of each group was used to calculate the tumor suppression rate (Fig. 8B). Compared with the vehicle treatment group, the tumor growth of the complexes-treated groups was significantly inhibited, and the tumor volumes of each complexes-treated groups were significantly reduced (Fig. 8C). The inhibition rates of complexes **5** and **6** on tumor growth were 50.8% and 47.6%, respectively, slightly lower than that of cisplatin (59%). At the same time, the body weight of mice treated with these two complexes did not decrease significantly, and the decreasing trend was smaller than that of cisplatin group, indicating that their toxicity was low (Fig. 8D).

2.12. Staining of tissues with TUNEL and H&E

Apoptosis of tumor tissues treated with complexes **5** and **6** was evaluated by TUNEL staining (Fig. 9A), which suggested that the apoptosis of tumor cells in complex **5** and **6** groups was significantly increased comparing with the control, and complex **5** showed stronger effect than complex **6**. Nuclear contraction was not obvious in any groups after DAPI staining.

Changes of Bax and Bcl-2 in tumor tissues of T-24 tumor-bearing mice were detected by Western blot (Fig. 9B and C). The results showed that in the T-24 xenograft tumor mouse model treated with complexes **5** and **6**, the expression level of Bcl-2 in group complex **5** was obviously decreased, while the change in group complex **6** was not obvious. However, the expression level of Bax in the two complex groups was increased, indicating that the ratio of Bcl/Bax was significantly decreased after the treatment of cells with complexes **5** and **6**. These results indicated that the complexes also induced apoptosis *in vivo*, which is consistent with the TUNEL staining results.

Histological examination of tumor tissues showed that the tumor cells in complexes **5** and **6** treated groups were closely arranged, round or polymorphic, with abundant cytoplasm, megakaryocytes, large and hyperchromatic nuclei. Compared with the control, there were more pyknotic tumor cells and fewer blood vessels in the tumor tissues of the complexes **5** and **6** treatment groups, indicating that tumor necrosis increased in the complexes **5** and **6** treatment groups. At the same time, the kidney, lung, spleen, liver and heart tissues of complexes **5** and **6** treated groups were similar to those of the vehicle group, and no obvious lesions were observed, indicating no obvious toxicity under the current treatment mode (Fig. 9D). In conclusion, complexes **5** and **6** exhibited strong inhibitory activity against proliferation *in vivo*.

3. Conclusion

Six rhodium(III) or palladium(II) complexes with pyrazolopyrimidines derivatives as ligands have been synthesized and characterized. Complexes **5** and **6** exhibited strong anticancer activity against several cancer cell lines and low toxicity against normal cells. Among the five rhodium complexes, complex **5** had the strongest activity when the pyrazole ring of the ligand contained phenyl group at the R_1 position, $-CH_3$ at the R_2 position, and hydrogen atom at the R_3 position. Complex **5** accumulated in mitochondria and nuclei and initiated a series of events associated with mitochondrial dysfunction and DNA damage, such as loss of MMP, ATP depletion, ROS release and elevated calcium levels, and cell cycle arrest, to induce ER stress response and subsequently apoptosis. Complexes **5** and **6** showed effective anticancer activity in a mouse tumor model. These compounds are potential promising anticancer metal complexes.

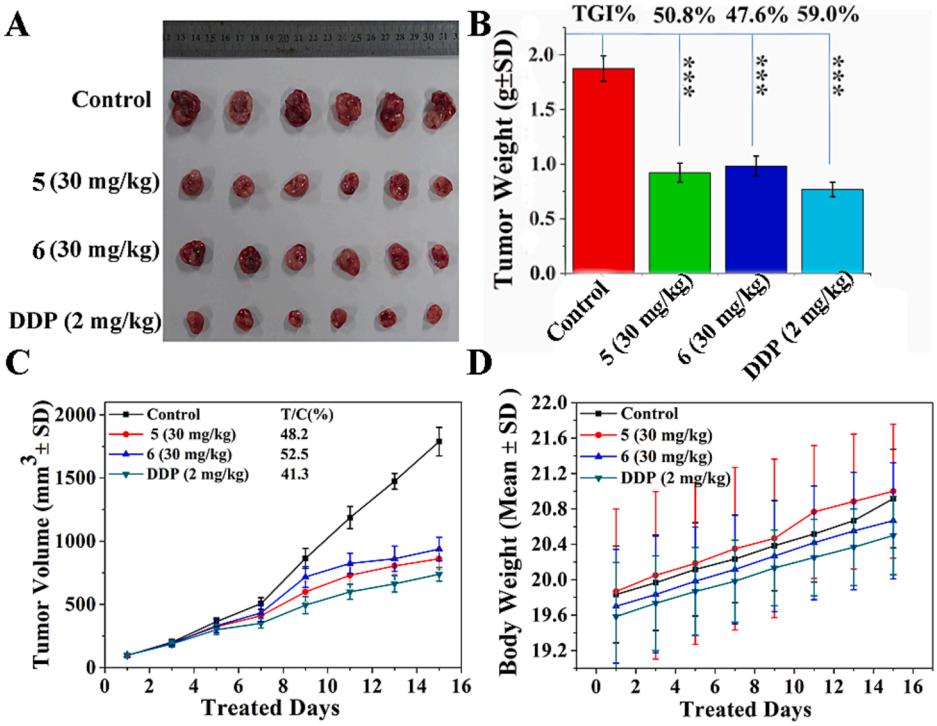

Fig. 8. Complexes **5** and **6** suppressed T-24 tumor growth *in vivo*. (A) Photographs of tumors separated from the mice. (B) Tumor weight was monitored. (C) Volume of tumors affected by **5** and **6** on T-24 tumor growth. (D) The body weight of the mice (n = 6) (***P < 0.001, **P < 0.01, *P < 0.05).

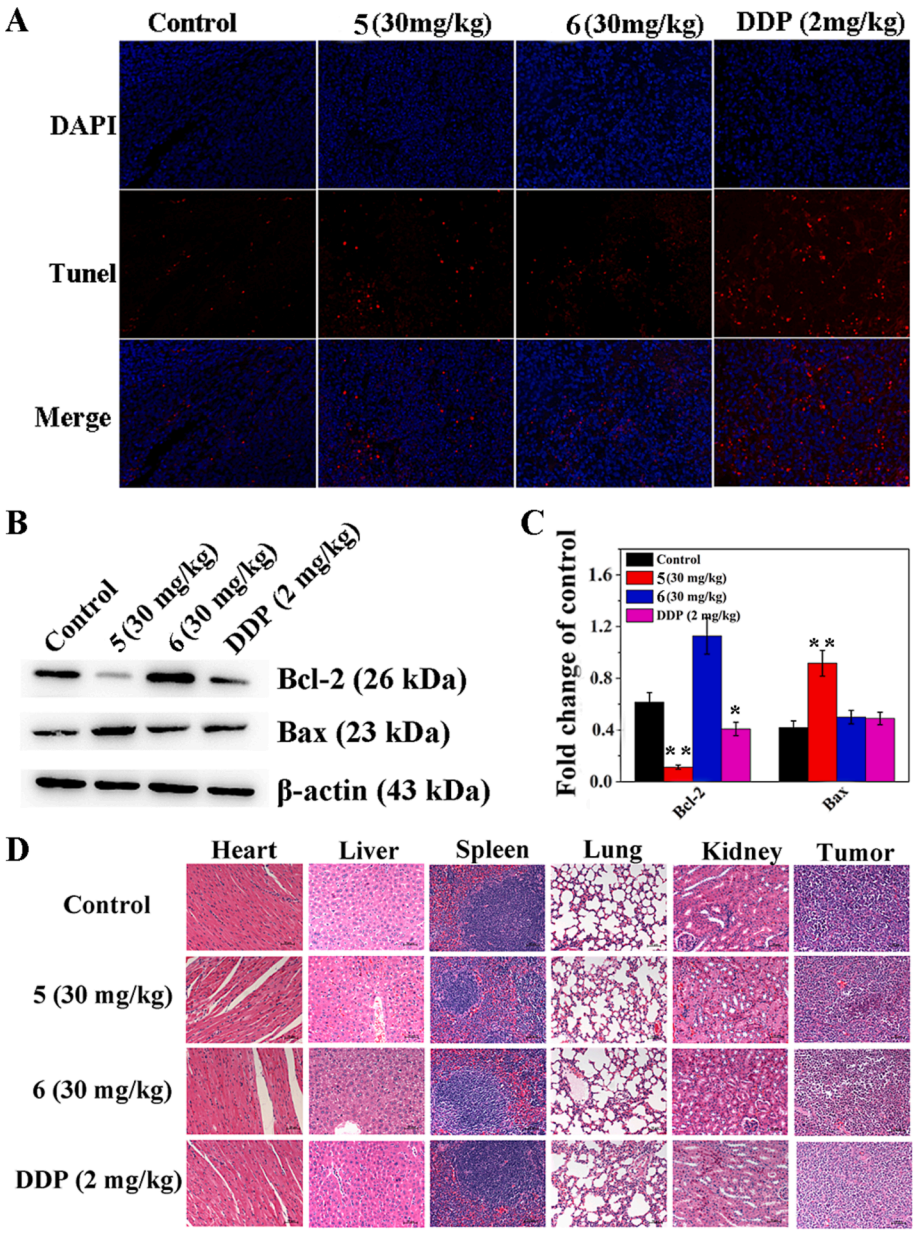

Fig. 9. (A) TUNEL staining of the tumor tissue treated with complexes **5** and **6**. (B) and (C) The change of apoptosis-related proteins after incubation of complexes **5** and **6** in tumor tissue. H&E staining of tumor tissue (D) and the visceral organ (E) of mice after complexes **5** and **6** treatment (200×) (***P < 0.001, **P < 0.01, *P < 0.05).

4. Experimental sections

4.1. Synthesis of ligands

Pyrazopyrimidine derivatives $\mathbf{L^{1-5}}$ and the complexes **1**–**6** were prepared using the previously reported method [24,66]. The structures of $\mathbf{L^{1-5}}$ and complexes **1**–**6** are shown in Scheme 1 and Scheme 2.

$\mathbf{L^2}$ (8-(3,5-diisopropyl-1H-pyrazol-1-yl)-2,4-diisopropyl-10-methylpyrido[2′,3′:3,4] pyrazolo[1,5-*a*]pyrimidine).

^{1}H NMR (400 MHz, Chloroform-*d*) δ 7.67 (d, 1H), 6.98 (s, 1H), 6.13 (s, 1H), 4.48 (p, 1H), 4.19 (p, 1H), 3.22 (p, 1H), 3.05 (s, 1H), 3.01 (d, 3H), 1.50 (d, 6H), 1.42 (d, 6H), 1.33 (d, 6H), 1.26 (d, 6H). ^{13}C NMR (151 MHz, Chloroform-*d*) δ 165.60, 160.13, 159.42, 156.15, 154.48, 153.62, 147.37, 143.87, 111.11, 105.80, 103.97, 102.32, 77.24, 77.03, 76.82, 36.41, 28.67, 28.13, 26.22, 22.77, 22.63, 22.11, 20.19, 19.00 (Fig. S1). HRMS (ESI) calcd for $C_{25}H_{34}N_6$ $[M + H]^+$ (*m/z*): 419.2923;

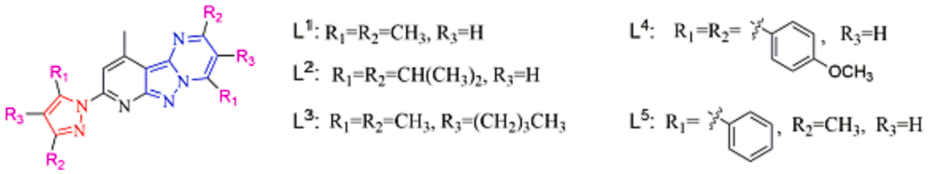

Scheme 1. The structures of ligands $\mathbf{L^{1-5}}$.

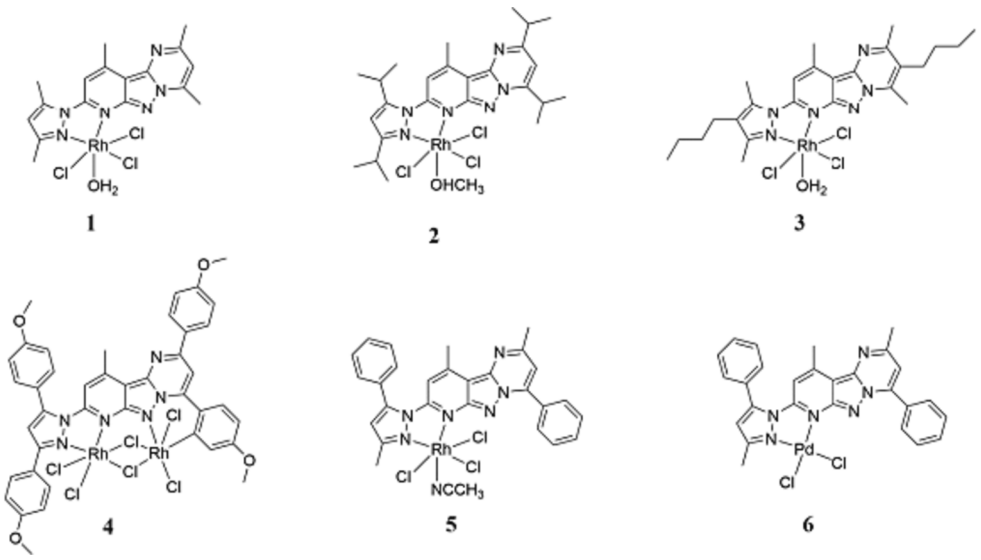

Scheme 2. The structures of complexes **1**–**6**.

Found, 419.2918 (Fig. S2). Anal. Calcd for $C_{25}H_{34}N_6$: C, 71.74; H, 8.19; N, 20.08. Found C, 71.59; H, 8.37; N, 19.84.

L^4 (8-(3,5-bis(4-methoxyphenyl)-1H-pyrazol-1-yl)-2,4-bis(4-methoxyphenyl)-10-methylpyrido[2′,3′:3,4]pyrazolo[1,5-a]pyrimidine).

^{1}H NMR (600 MHz, DMSO-d_6) δ 8.45 (d, 2H), 8.31 (d, 2H), 8.20 (s, 1H), 7.91 (d, 2H), 7.54 (s, 1H), 7.29 (d, 2H), 7.17 (t, 4H), 7.10 (s, 1H), 7.04 (d, 2H), 6.89 (d, 2H), 3.88 (s, 6H), 3.81 (s, 3H), 3.72 (s, 3H), 3.11 (s, 3H). (Fig. S3) HRMS (ESI) calcd for $C_{41}H_{34}N_6O_4$ $[M + H]^+$ (*m/z*): 675.2720; Found, 675.2685 (Fig. S4). Anal. Calcd for $C_{41}H_{34}N_6O_4$: C, 72.98; H, 5.08; N, 12.46. Found C, 72.75; H, 5.36; N, 12.30.

4.2. Synthesis and characterization of complexes 1–6

Synthesis of rhodium complexes 1–6: Ligands **L^{1-5}** (0.1 mmol, 1 equiv.) and $RhCl_3{\cdot}3H_2O$] (0.12 mmol, 1.2 equiv.) were added to $CHCl_3$:CH_3OH or $CHCl_3$:CH_3CN (complex **5**) (v:v = 2:1, 9.0 mL) for reflux for 10 h. After filtration and standing for 5 d, red brown block crystals suitable for single crystal X-ray diffraction analysis were collected. Complex **6** was obtained by replacing $RhCl_3{\cdot}3H_2O$ with $PdCl_2$ and reacted with ligand **L^5** under the same reaction conditions.

[Rh(L^1)(H_2O)Cl_3] (1): Yellow block crystal. Yield: 62%. ^{1}H NMR (600 MHz, DMSO-d_6) δ 7.64 – 7.64 (m, 1H), 7.62 (s, 1H), 6.68 (s, 1H), 3.17 (s, 1H), 3.12 (s, 3H), 2.96 (s, 3H), 2.93 (s, 3H), 2.78 (s, 3H), 2.75 (s, 3H). ^{13}C NMR (151 MHz, DMSO-d_6) δ 160.09, 159.61, 155.49, 152.94, 152.69, 146.37, 145.84, 143.34, 114.80, 114.78, 105.48, 105.28, 48.63, 40.06, 39.94, 39.92, 39.80, 39.66, 39.52, 39.38, 39.29, 39.24, 39.10, 24.42, 18.84, 18.09, 15.17, 14.76 (Fig. S5). HRMS (ESI) calcd for $C_{17}H_{20}Cl_3N_6ORh$ $[M-Cl-H_2O]^+$ (*m/z*): 497.0131; Found, 497.0562 (Fig. S6). Anal. Calcd for $C_{17}H_{20}Cl_3N_6ORh$: C, 38.26; H, 3.78; N, 15.75. Found C, 38.09; H, 3.66; N, 15.93.

[Rh(L^2)(CH_3OH)Cl_3] (2): Yellow block crystal. Yield: 59%. ^{1}H NMR (600 MHz, DMSO-d_6) δ 7.65–7.64 (m, 1H), 7.62 (s, 1H), 6.88 (s, 1H), 4.39–4.36 (m, 1H), 3.97 (dt, J = 33.0, 6.7 Hz, 3H), 3.17–3.14 (m, 3H), 2.08 (s, 3H), 1.53 (d, J = 6.9 Hz, 6H), 1.41 (d, J = 3.0 Hz, 6H), 1.40 (d, J = 3.3 Hz, 6H), 1.29 (d, J = 6.9 Hz, 6H). ^{13}C NMR (151 MHz, DMSO-d_6) δ 170.01, 168.53, 156.95, 155.56, 155.03, 153.05, 152.84, 143.39, 118.14, 108.98, 108.06, 106.02, 105.58, 40.06, 39.94, 39.80, 39.66, 39.52, 39.38, 39.24, 39.10, 35.68, 28.78, 26.93, 26.20, 22.62, 22.61, 21.94, 21.75, 21.73, 19.86, 18.69 (Fig. S7). HRMS (ESI) calcd for $C_{26}H_{38}Cl_3N_6ORh$, [M + DMSO + H]$^+$ (*m/z*): 737.1445, Found, 737.0673 ; $[M + H]^+$ (*m/z*): 659.1306, Found, 659.1990 (Fig. S8). Anal. Calcd for $C_{26}H_{38}Cl_3N_6ORh$: C, 47.32; H, 5.80; N, 12.74. Found C, 47.06; H, 5.68; N, 12.61.

[Rh(L^3)(H_2O)Cl_3] (3): Yellow block crystal. Yield: 51%. ^{1}H NMR (600 MHz, DMSO-d_6) δ 7.63–7.62 (m, 1H), 3.12–3.10 (m, 3H), 2.96 (s, 3H), 2.92–2.89 (m, 2H), 2.88 (s, 3H), 2.79 (s, 3H), 2.76 (s, 3H), 2.56 (t, J = 7.6 Hz, 2H), 1.56 (dq, J = 5.9, 3.2, 2.7 Hz, 2H), 1.50–1.44 (m, 4H), 1.40 – 1.34 (m, 2H), 0.97 (t, J = 7.3 Hz, 3H), 0.94 (t, J = 7.3 Hz, 3H). ^{13}C NMR (151 MHz, DMSO-d_6) δ 159.32, 158.86, 155.37, 152.78, 152.04, 144.11, 142.30, 141.31, 125.99, 124.66, 105.42, 105.34, 40.06, 39.94, 39.80, 39.66, 39.52, 39.38, 39.24, 39.10, 31.72, 31.03, 27.71, 23.53, 22.24, 22.09, 21.78, 18.73, 15.04, 13.85, 13.76, 13.31, 12.99 (Fig. S9). HRMS (ESI) calcd for $C_{25}H_{36}Cl_3N_6ORh$, [M + DMSO-Cl]$^+$ (*m/z*): 687.1522, Found, 687.1472 ; $[M + CH_3CN + DMSO\text{-}H_2O\text{-}Cl]^+$ (*m/z*): 710.1682, Found, 710.1138 (Fig. S10). Anal. Calcd for $C_{25}H_{36}Cl_3N_6ORh$: C, 46.49; H, 5.62; N, 13.01. Found C, 46.68; H, 5.40; N, 13.27.

[Rh_2(L^4)Cl_6] ·CH_3OH (4): Yellow block crystal. Yield: 75%. HRMS (ESI) calcd for $C_{42}H_{37}Cl_6N_6O_5Rh_2$, $[M + CH_3CN + CH_3OH + H]^+$ (*m/z*): 1165.9459, Found, 1165.8799 ; $[M + CH_3CN + CH_3OH\text{-}Cl]^+$ (*m/z*): 1129.9692, Found, 1129.9768 (Fig. S11). Anal. Calcd for $C_{42}H_{37}Cl_6N_6O_5Rh_2$: C, 44.87; H, 3.32; N, 7.48. Found C, 44.73; H, 3.48; N, 7.29.

[Rh(L^5)(CH_3CN)Cl_3] ·0.5CH_3CN (5): Yellow block crystal. Yield: 83%. ^{1}H NMR (400 MHz, DMSO-d_6) δ 8.17–8.12 (m, 2H), 7.76–7.69 (m, 8H), 7.64 (d, J = 1.8 Hz, 1H), 7.02 (s, 1H), 6.46 (s, 1H), 3.17 (s, 3H), 2.79 (s, 3H), 2.77 (d, J = 1.8 Hz, 3H), 2.75 (s, 3H). ^{13}C NMR (101 MHz, DMSO-d_6) δ 160.66, 160.44, 155.80, 153.10, 151.51, 148.09, 146.07, 144.44, 131.39, 131.08, 130.43, 130.02, 129.74, 129.35, 128.99, 128.90, 128.53, 115.58, 114.80, 106.86, 105.24, 48.61, 24.38, 18.94, 14.38 (Fig. S12). HRMS (ESI) calcd for $C_{30}H_{26.5}Cl_3N_{7.5}Rh$, $[M-1.5CH_3CN + H]^+$ (*m/z*): 641.0075, Found, 641.1432 ; [M + DMSO + H_2O-0.5CH_3CN-Cl]$^+$ (*m/z*): 740.0849, Found, 740.0044 (Fig. S13). Anal. Calcd for $C_{30}H_{26.5}Cl_3N_{7.5}Rh$: C, 51.38; H, 3.81; N, 14.98. Found C, 51.23; H, 3.69; N, 15.16.

[Pd(L^5)Cl_2] (6): Yellow block crystal. Yield: 78%. ^{1}H NMR (600 MHz, DMSO-d_6) δ 8.12–8.09 (m, 2H), 7.67 (s, 1H), 7.62–7.58 (m, 3H), 7.49 (s, 1H), 7.28–7.24 (m, 5H), 6.53 (s, 1H), 3.00 (s, 3H), 2.76 (s, 8H), 2.32 (s, 3H) (Fig. S14). HRMS (ESI) calcd for $C_{27}H_{22}Cl_2N_6Pd$, $[M-Cl]^+$ (*m/z*): 571.0629; Found, 571.0613; $M-Cl + DMSO]^+$ (*m/z*): 651.0773; Found, 651.0740 (Fig. S15). Anal. Calcd for $C_{27}H_{22}Cl_2N_6Pd$: C, 53.35; H, 3.65; N, 13.83. Found C, 53.09; H, 3.86; N, 13.65.

4.3. Cellular uptake of complexes

The cells were incubated in 100 mm cell culture dishes for overnight, and then treated with complexes **5** and **6** (10 μM) for 24 h. After the cells were collected, washed, harvested, and digested with HNO_3, the metal content in the diluent was detected by ICP-MS. The cytoplasm, mitochondria, and cell membrane were isolated, digested with concentrated HNO_3, and their metal contents were determined by ICP-MS.

4.4. Detection of cell cycle

T-24 cells (1×10^6 cells/dish) in 70 mm dish were treated with complexes **5** (2.0, 3.0, 4.0 μM) and **6** (4.0 μM) for 24 h. The cells were collected and washed with PBS. Ice-cold ethanol and PBS were added drop by drop while shaking, and then fixed in 70% ethanol in −20 °C refrigerator for 24 h. The cells were centrifuged, washed with PBS, and incubated with dye in 5% CO_2 humidified environment at 37 °C for 30 min, and then tested by flow cytometry.

4.5. Assessment of apoptosis

T-24 cells (2×10^5 cells/well) were cultured in 6-well plates overnight. After treatment with complexes **5** (2.0, 3.0, 4.0 μM) and **6** (4.0 μM) for 24 h and 48 h, respectively, the cells were harvested, washed and incubated with PI (5.0 μL) and annexin V (5.0 μL) in a 5% CO_2 humidified environment for 30 min. Cell apoptosis was determined by flow cytometry.

4.6. Detection of intracellular ATP level

After T-24 tumor cells were treated with complex **5** for 24 h, the cells were fully lysed and centrifuged at 12,000 g for 5 min. Subsequently, 100 μL of ATP assay working diluent was added to the 96 well in advance, followed by adding 20 μL of cell lysis supernatant to the 96 well, then the fast well. The wells were rapidly mixed, and their luminance values were immediately measured by a cell imaging multimode reader.

4.7. Anticancer activity in vivo

T-24 (5×10^6 cells per mouse) cells in the exponential growth state were injected into mice (Balb/c nude mice) by subcutaneous injection to create a tumor model. The successfully modeled mice were divided into 3 groups (n = 6): vehicle group, complex **5** (30 mg/kg) and complex **6** (30 mg/kg) groups. The vehicle (control) group was treated with normal saline (v/v) containing 5% DMSO. Tumor diameter and weight were measured the next day, and the mice were sacrificed after 15 days of continued treatment. Tumor specimens were collected and weighed, embedded in paraffin and fixed with formalin.

4.8. Other experimental procedures

Details of other experiments not described here are provided in the suplementary documents, such as single crystal X-ray diffraction analysis, stability and purity test by HPLC spectra and UV-Vis spectra, detection of lipophilicity, *in vitro* cytotoxicity assay, studies of whole genome sequencing, comet assay, mitochondrial membrane potential analysis, ROS and Ca^{2+} generation, determination of Caspase 3, Caspase 8 and Caspase 9, Western Blot analysis, acute toxicity study, H&E and TUNEL staining. CCDC reference numbers of complexes **1**–**6** were 2,215,625 (complex **1**), 2,215,651 (complex **2**), 2,215,652 (complex **3**), 2,215,653 (complex **4**), 2,215,654 (complex **5**) 2,215,655 (complex **6**), respectively. The biological experiments were carried out in the absence of light, and the compounds were stable in dimethylsulfoxide.

4.9. Statistical studies

All experiments were repeated three times and the data were expressed as mean ± standard deviation (SD).

Declaration of Competing Interest

The authors declare that they have no known competing financial interests or personal relationships that could have appeared to influence the work reported in this paper.

Data availability

Data will be made available on request.

Acknowledgments

This work was supported by the National Natural Science Foundation of China (Grant: 22077022) and Natural Science Foundation of Guangxi Province of China (Grants: GUIKEZY22096015, 2023GXNSFDA026054).

Appendix A. Supplementary data

Supplementary data to this article can be found online at https://doi.org/10.1016/j.bioorg.2023.106838.

References

[1] F. Bray, M. Laversanne, E. Weiderpass, I. Soerjomataram, The ever-increasing importance of cancer as a leading cause of premature death worldwide, Cancer 127 (2021) 3029–3030.
[2] T. Yan, X. Zheng, S. Liu, Y. Zou, J. Liu, Ion transporters: emerging agents for anticancer therapy, Science China. Chemistry 65 (2022) 1265–1278.
[3] J. Zang, B. Zhang, Y. Wang, X. Wang, S. Gou, Design, synthesis and biological evaluation of antitumor platinum(II) agents conjugated with non-steroidal anti-inflammatory drug species, Bioorganic Chemistry 120 (2022) 105633–105643.
[4] H. Zhang, M. Zhang, Y. Zhang, H. Wang, L. Zhao, H. Xu, Activatable fluorescence molecular imaging and anti-tumor effects investigation of GSH-sensitive BRD4 ligands, Bioorganic Chemistry 120 (2022) 105636–105645.
[5] T. Wang, Q. Meng, L. Lin, L. Yang, W. Zhao, D. Sun, Self-assembled dehydropeptide nanocarrier as a delivery system for antitumor drug temozolomide, Bioorganic Chemistry 124 (2022) 105842–105850.
[6] C. Orvig, M.J. Abrams, Medicinal inorganic chemistry: Introduction, Chemical Reviews 99 (1999) 2201–2204.
[7] M. Zhang, H. Yu, J. Hu, Z. Zhao, L. Liu, G. Yang, T. Wang, G. Han, S. Song, Therapeutic carrier based on solanesol and hyaluronate for synergistic tumor treatment, International Journal of Biological Macromolecules 201 (2022) 20–28.
[8] L. Li, J. Yu, S. Cheng, Z. Peng, H. Luo, Transcription factor Fli-1 as a new target for antitumor drug development, International Journal of Biological Macromolecules 209 (2022) 1155–1168.
[9] M. Valipour, Recent advances of antitumor shikonin/alkannin derivatives: A comprehensive overview focusing on structural classification, synthetic approaches, and mechanisms of action, European Journal of Medicinal Chemistry 235 (2022) 114314–114369.
[10] H. Duan, A.G.A. Er-bu, Z. Dongzhi, H. Xie, B. Ye, J. He, Alkaloids from Dendrobium and their biosynthetic pathway, biological activity and total synthesis, Phytomedicine 102 (2022) 154132–154148.
[11] S. Moradi, R. Najjar, H. Hamishehkar, A. Lotfi, Triple-responsive drug nanocarrier: Magnetic core-shell nanoparticles of Fe3O4@poly(N-isopropylacrylamide)-grafted-chitosan, synthesis and in vitro cytotoxicity evaluation against human lung and breast cancer cells, J. Drug. Deliv. Sci. Tec. 72 (2022) 103426–103436.
[12] J. Kasparkova, H. Kostrhunova, V. Novohradsky, C. Logvinov capital, A.V. V. Temnov, N.E. Borisova, T.A. Podrugina, L. Markova, P. Starha, A.A. Nazarov, V. Brabec, Novel cis-Pt(II) complexes with alkylpyrazole ligands: Synthesis, characterization, and unusual mode of anticancer action, Bioinorganic Chemistry and Applications 2022 (2022) 1717200–1717212.
[13] A.C. Flick, C.A. Leverett, H.X. Ding, E.L. McInturff, S.J. Fink, S. Mahapatra, D. W. Carney, E.A. Lindsey, J.C. DeForest, S.P. France, S. Berritt, S.V. Bigi-Botterill, T. S. Gibson, R.B. Watson, Y. Liu, C.J. O'Donnell, Synthetic approaches to the new drugs approved during 2020, Journal of Medicinal Chemistry 65 (2022) 9607–9661.
[14] S.M. Hassona, E.A. Saad, H.A. Kiwan, M.M. Hassanien, Palladium(II) Schiff base complex arrests cell cycle at early stages, induces apoptosis, and reduces Ehrlich solid tumor burden: a new candidate for tumor therapy, Investigational New Drugs 40 (4) (2022) 681–689.

[15] N. Toupin, M.K. Herroon, R.P. Thummel, C. Turro, I. Podgorski, H. Gibson, J. J. Kodanko, Metalloimmunotherapy with rhodium and ruthenium complexes: Targeting tumor-associated macrophages, Chemistry 28 (2022) e202104430–e202104440.
[16] D. Simic, M. Zaric, I. Nikolic, R. Zivkovic-Zaric, P. Canovic, A. Kocovic, I. Radojevic, I. Rakovic, S. Jovicic Milic, D. Petrovic, D. Stojkovic, N. Vukovic, M. Kacaniova, M. Vukic, V. Jevtic, Newly synthesized palladium(II) complexes with aminothiazole derivatives: In vitro study of antimicrobial activity and antitumor activity on the human prostate cancer cell line, Dalton Transactions 51 (2022) 1191–1205.
[17] C.-H. Leung, H.-J. Zhong, D.-S.-H. Chan, D.-L. Ma, Bioactive iridium and rhodium complexes as therapeutic agents, Coordination Chemistry Reviews 257 (2013) 1764–1776.
[18] A. Nahaei, Z. Mandegani, S. Chamyani, M. Fereidoonnezhad, H.R. Shahsavari, N. Y. Kuznetsov, S.M. Nabavizadeh, Half-Sandwich cyclometalated Rh(III) complexes bearing thiolate ligands: Biomolecular interactions and in vitro and in vivo evaluations, Inorganic Chemistry 61 (2022) 2039–2056.
[19] J. Gao, L. Guo, Y. Wu, Y. Cheng, X. Hu, J. Liu, Z. Liu, 16-Electron half-sandwich rhodium(III), iridium(III), and ruthenium(II) complexes as lysosome-targeted anticancer agents, Organometallics 40 (2021) 3999–4010.
[20] J. Wang, J.J. Nie, P. Guo, Z. Yan, B. Yu, W. Bu, Rhodium(I) complex-based polymeric nanomicelles in water exhibiting coexistent near-infrared phosphorescence imaging and anticancer activity in vivo, Journal of the American Chemical Society 142 (2020) 2709–2714.
[21] J.J. Zhang, J.K. Muenzner, M.A. Abu El Maaty, B. Karge, R. Schobert, S. Wolfl, I. Ott, A multi-target caffeine derived rhodium(I) N-heterocyclic carbene complex: evaluation of the mechanism of action, Dalton Transactions 45 (2016) 13161–13168.
[22] S. Nasiri Sovari, F. Zobi, Recent studies on the antimicrobial activity of transition metal complexes of groups 6–12, Chemistry 2 (2020) 418–452.
[23] D. Tesauro, Metal complexes in diagnosis and therapy, International Journal of Molecular Sciences 23 (2022) 4377–4380.
[24] Y.Q. Gu, K. Yang, Q.Y. Yang, H.Q. Li, M.Q. Hu, M.X. Ma, N.F. Chen, Y.H. Liu, H. Liang, Z.-F. Chen, Rhodium(III)-picolinamide complexes act as anti-cancer and anti-metastasis agent via inducing apoptosis and autophagy, Journal of Medicinal Chemistry 66 (2023) 9592–9606.
[25] F. Hackenberg, L. Oehninger, H. Alborzinia, S. Can, I. Kitanovic, Y. Geldmacher, M. Kokoschka, S. Wölfl, I. Ott, W.S. Sheldrick, Highly cytotoxic substitutionally inert rhodium(III) tris(chelate) complexes: DNA binding modes and biological impact on human cancer cells, Journal of Inorganic Biochemistry 105 (7) (2011) 991–999.
[26] H.A. Sahyon, F. Althobaiti, A.-E.-M.-M. Ramadan, A.M. Fathy, Quercetin-based rhodium(III) complex: Synthesis, characterization and diverse biological potentials, Journal of Molecular Structure 1257 (2022) 132584–132598.
[27] A. Goudarzi, M. Ghassemzadeh, M. Saeidifar, K. Aghapoor, F. Mohsenzadeh, B. Neumüller, In vitro cytotoxicity and antibacterial activity of [Pd(AMTTO)(PPh3)2]: a novel promising palladium(II) complex, New Journal of Chemistry 46 (2022) 3026–3034.
[28] N.S. Gul, T.-M. Khan, Y.-C. Liu, M.I. Choudhary, Z.-F. Chen, H. Liang, Pd(II) and Rh (III) complexes with isoquinoline derivatives induced mitochondria-mediated apoptotic and autophagic cell death in HepG2 cells, CCS Chem. 3 (6) (2021) 1626–1641.
[29] Y.Q. Gu, W.Y. Shen, Q.Y. Yang, Z.-F. Chen, H. Liang, Ru(III) complexes with pyrazolopyrimidines as anticancer agents: bioactivities and the underlying mechanisms, Dalton Transactions 51 (2022) 1333–1343.
[30] V. Asati, A. Anant, P. Patel, K. Kaur, G.D. Gupta, Pyrazolopyrimidines as anticancer agents: A review on structural and target-based approaches, European Journal of Medicinal Chemistry 225 (2021) 13781–13811.
[31] G.S. Hassan, D.E. Abdel Rahman, Y.M. Nissan, E.A. Abdelmajeed, T. M. Abdelghany, Novel pyrazolopyrimidines: Synthesis, in vitro cytotoxic activity and mechanistic investigation, European Journal of Medicinal Chemistry 138 (2017) 565–576.
[32] Q.Y. Yang, R. Ma, Y.Q. Gu, X.F. Xu, Z.-F. Chen, H. Liang, Arene-ruthenium(II)/osmium(II) complexes potentiate the anticancer efficacy of metformin via glucose metabolism reprogramming, Angewandte Chemie, International Edition 61 (2022) e202208570.
[33] W.Y. Shen, C.P. Jia, L.Y. Liao, L.L. Chen, C. Hou, Y.H. Liu, H. Liang, Z.-F. Chen, Copper(II) complexes of halogenated quinoline Schiff base derivatives enabled cancer Therapy through glutathione-assisted chemodynamic therapy and inhibition of autophagy flux, Journal of Medicinal Chemistry 65 (2022) 5134–5148.
[34] A. Santos, J.X. Soares, S. Cravo, M.E. Tiritan, S. Reis, C. Afonso, C. Fernandes, M.M. M. Pinto, Lipophilicity assessment in drug discovery: Experimental and theoretical methods applied to xanthone derivatives, Journal of Chromatography. B, Analytical Technologies in the Biomedical and Life Sciences 1072 (2018) 182–192.
[35] F. Mello-Andrade, A.P.M. Guedes, W.C. Pires, V.S. Velozo-Sa, K.A. Delmond, D. Mendes, M.S. Molina, L. Matuda, M.A.M. de Sousa, P. Melo-Reis, C.C. Gomes, C. H. Castro, M.A.P. Almeida, C.F.M. Menck, A.A. Batista, R. Burikhanov, V. M. Rangnekar, E. Silveira-Lacerda, Ru(II)/amino acid complexes inhibit the progression of breast cancer cells through multiple mechanism-induced apoptosis, Journal of Inorganic Biochemistry 226 (2022) 111625–111636.
[36] K. Xiong, C. Qian, Y. Yuan, L. Wei, X. Liao, L. He, T.W. Rees, Y. Chen, J. Wan, L. Ji, H. Chao, Necroptosis induced by ruthenium(II) complexes as dual catalytic inhibitors of topoisomerase I/II, Angewandte Chemie, International Edition 59 (2020) 16631–16637.
[37] F.Y. Wang, X.M. Tang, X. Wang, K.B. Huang, H.W. Feng, Z.F. Chen, Y.N. Liu, H. Liang, Mitochondria-targeted platinum(II) complexes induce apoptosis-dependent autophagic cell death mediated by ER-stress in A549 cancer cells, European Journal of Medicinal Chemistry 155 (2018) 639–650.
[38] Y. Guo, S. Jin, H. Yuan, T. Yang, K. Wang, Z. Guo, X. Wang, DNA-unresponsive platinum(II) complex induces ERS-mediated mitophagy in cancer cells, Journal of Medicinal Chemistry 65 (2022) 520–530.
[39] S.J. Thompson, A. Rooney, K.M. Prise, S.J. McMahon, Evaluating iodine-125 DNA damage benchmarks of monte carlo DNA damage models, Cancers 14 (2022) 14030463–14030478.
[40] L.F. McSwain, K.K. Parwani, S.W. Shahab, D. Hambardzumyan, T.J. MacDonald, J. M. Spangle, A.M. Kenney, Medulloblastoma and the DNA damage response, Front, Oncol. 12 (2022) 903830–903846.
[41] A.O. Abotaleb, R.A. Zinhoum, A. Gabarty, Evaluation of irradiation quarantine dose-induced DNA damage in Rhyzopertha dominica and its effect on wheat grains using comet assay, Int. J. Trop. Insect. Sc. 41 (1) (2021) 693–701.
[42] X.L. Song, Y.J. Zhang, X.F. Wang, W.J. Zhang, Z. Wang, F. Zhang, Y.J. Zhang, J. H. Lu, J.W. Mei, Y.P. Hu, L. Chen, H.F. Li, Y.Y. Ye, Y.B. Liu, J. Gu, Casticin induces apoptosis and G0/G1 cell cycle arrest in gallbladder cancer cells, Cancer Cell International 17 (2017) 9–18.
[43] M. Zhang, Q. Lu, H. Hou, D. Sun, M. Chen, F. Ning, P. Wu, D. Wei, Y. Duan, Y. Pan, G. Lash, Garcinol inhibits the proliferation of endometrial cancer cells by inducing cell cycle arrest, Oncology Reports 45 (2020) 630–640.
[44] J. Li, P. Zhu, Y. Chen, S. Zhang, Z. Zhang, Z. Zhang, Y. Wang, X. Jiang, K. Lin, W. Wu, Z. Mo, S.C.W. Sze, K.K.L. Yung, Isoalantolactone induces cell cycle arrest, apoptosis and autophagy in colorectal cancer cells, Frontiers in Pharmacology 13 (2022) 903599–903613.
[45] J.K. Buolamwini, Cell cycle molecular targets in novel anticancer drug discovery, Current Pharmaceutical Design 6 (2000) 379–392.
[46] H. Yao, S. Xie, X. Ma, J. Liu, H. Wu, A. Lin, H. Yao, D. Li, S. Xu, D.H. Yang, Z. S. Chen, J. Xu, Identification of a potent oridonin analogue for treatment of triple-negative breast cancer, Journal of Medicinal Chemistry 63 (2020) 8157–8178.
[47] Y.B. Peng, W. He, Q. Niu, C. Tao, X.L. Zhong, C.P. Tan, P. Zhao, Mitochondria-targeted cyclometalated rhodium(III) complexes: Synthesis, characterization and anticancer research, Dalton Transactions 50 (2021) 9068–9075.
[48] Q.i. Xie, X. Fan, Y. Han, B.-X. Wu, B. Zhu, Daphnoretin arrests the cell cycle and induces apoptosis in human breast cancer cells, Journal of Natural Products 85 (10) (2022) 2332–2339.
[49] R.C. Scaduto, L.W. Grotyohann, Measurement of mitochondrial membrane potential using fluorescent rhodamine derivatives, Biophysical Journal 76 (1999) 469–477.
[50] A. Erxleben, Mitochondria-targeting anticancer metal complexes, Current Medicinal Chemistry 26 (2019) 694–728.
[51] X.Y. Fan, X.Y. Chen, Y.J. Liu, H.M. Zhong, F.L. Jiang, Y. Liu, Oxidative stress-mediated intrinsic apoptosis in human promyelocytic leukemia HL-60 cells induced by organic arsenicals, Scientific Reports 6 (2016) 29865–29876.
[52] X. Chen, L.u. Liu, P. Liu, Y. Chen, D. Lin, H. Yan, Q.i. Yan, Y.i. Wang, Y. Qiu, B. o. Fang, H. Huang, J. Qian, Y. Zhao, Z. Du, Q. Zhang, X. Li, X. Zheng, Z. Liu, Discovery of potent and orally bioavailable platelet-derived growth factor receptor (PDGFR) inhibitors for the treatment of osteosarcoma, Journal of Medicinal Chemistry 65 (7) (2022) 5374–5391.
[53] N. Gong, X. Ma, X. Ye, Q. Zhou, X. Chen, X. Tan, S. Yao, S. Huo, T. Zhang, S. Chen, X. Teng, X. Hu, J. Yu, Y. Gan, H. Jiang, J. Li, X.-J. Liang, Carbon-dot-supported atomically dispersed gold as a mitochondrial oxidative stress amplifier for cancer treatment, Nature Nanotechnology 14 (4) (2019) 379–387.
[54] B. Gottschalk, Z. Koshenov, M. Waldeck-Weiermair, S. Radulovic, F.E. Oflaz, M. Hirtl, O.A. Bachkoenig, G. Leitinger, R. Malli, W.F. Graier, MICU1 controls spatial membrane potential gradients and guides Ca(2+) fluxes within mitochondrial substructures, Commun. Biol. 5 (2022) 649–661.
[55] X. Cui, Y. Zhang, Y. Lu, M. Xiang, ROS and Endoplasmic Reticulum Stress in Pulmonary Disease, Frontiers in Pharmacology 13 (2022) 879204–879218.
[56] X. Li, J. Zhu, Q. Lin, M. Yu, J. Lu, J. Feng, C. Hu, Effects of curcumin on mitochondrial function, endoplasmic reticulum stress, and mitochondria-associated endoplasmic reticulum membranes in the jejunum of oxidative stress piglets, Journal of Agricultural and Food Chemistry 70 (2022) 8974–8985.
[57] N. Ebrahimi, J. Saremi, M. Ghanaatian, E. Yazdani, S. Adelian, S. Samsami, N. Moradi, N. Rostami Ravari, A. Ahmadi, M.R. Hamblin, A.R. Aref, The role of endoplasmic reticulum stress in the regulation of long noncoding RNAs in cancer, Journal of Cellular Physiology 237 (2022) 3752–3767.
[58] S. Orrenius, B. Zhivotovsky, P. Nicotera, Regulation of cell death: The calcium-apoptosis link, Nature Reviews. Molecular Cell Biology 4 (7) (2003) 552–565.
[59] L. Fan, B. Song, G. Sun, T. Ma, F. Zhong, W. Wei, G. Velasco, Endoplasmic reticulum stress-induced resistance to doxorubicin is reversed by paeonol treatment in human hepatocellular carcinoma cells, PLoS One1 8 (5) (2013) e62627.
[60] R. Cao, J. Jia, X. Ma, M. Zhou, H. Fei, Membrane localized iridium(III) complex induces endoplasmic reticulum stress and mitochondria-mediated apoptosis in human cancer cells, Journal of Medicinal Chemistry 56 (2013) 3636–3644.
[61] C. Huang, T. Li, J. Liang, H. Huang, P. Zhang, S. Banerjee, Recent advances in endoplasmic reticulum targeting metal complexes, Coordination Chemistry Reviews 408 (2020) 213178–213192.
[62] D. Fei, H. Zhao, Y. Wang, J. Liu, M. Mu, M. Guo, X. Yang, M. Xing, The disturbance of autophagy and apoptosis in the gizzard caused by copper and/or arsenic are related to mitochondrial kinetics, Chemosphere 231 (2019) 1–9.

[63] H. Yamaguchi, H.G. Wang, CHOP is involved in endoplasmic reticulum stress-induced apoptosis by enhancing DR5 expression in human carcinoma cells, The Journal of Biological Chemistry 279 (2004) 45495–45502.
[64] A. Jangra, M. Verma, D. Kumar, M. Chandrika, A. Rachamalla, K. Dey, S.K. Dua, S. Jha, A. Ojha, D. Alexiou, N.K.J.a. Kumar, Targeting endoplasmic reticulum stress using natural products in neurological disorders, Neuroscience and Biobehavioral Reviews 141 (2022) 104818–104840.
[65] X. Duan, Y. Liao, T. Liu, H. Yang, Y. Liu, Y. Chen, R. Ullah, T. Wu, Zinc oxide nanoparticles synthesized from cardiospermum halicacabum and its anticancer activity in human melanoma cells (A375) through the modulation of apoptosis pathway, Journal of Photochemistry and Photobiology. B 202 (2020) 111718–111727.
[66] Y.Q. Gu, W.Y. Shen, Y. Zhou, S.F. Chen, Y. Mi, B.F. Long, D.J. Young, F.L. Hu, A pyrazolopyrimidine based fluorescent probe for the detection of Cu(2+) and Ni(2+) and its application in living cells, Spectrochim Acta A Mol. Biomol, Spectrosc. 209 (2019) 141–149.